

Structure and Binding in Halide Perovskites: Analysis of Static and Dynamic Effects from Dispersion-Corrected Density Functional Theory

H. Beck,¹ C. Gehrman,¹ and D. A. Egger^{1, a)}

Institute of Theoretical Physics, University of Regensburg, Universitätsstraße 31, 93053 Regensburg

(Dated: 21 November 2021)

We investigate the impact of various levels of approximation in density functional theory calculations for the structural and binding properties of the prototypical halide perovskite MAPbI₃. Specifically, we test how the inclusion of different correction schemes for including dispersive interactions, and how in addition using hybrid density functional theory, affects the results for pertinent structural observables by means of comparison to experimental data. In particular, the impact of finite temperature on the lattice constants and bulk modulus, and the role of dispersive interactions in calculating them, is examined by using molecular dynamics based on density functional theory. Our findings confirm previous theoretical work showing that including dispersive corrections is crucial for accurate calculation of structural and binding properties of MAPbI₃. They furthermore highlight that using a computationally much more expensive hybrid density functional has only minor consequences for these observables. This allows for suggesting the use of semilocal density functional theory, augmented by pairwise dispersive corrections, as a reasonable choice for structurally more complicated calculations of halide perovskites. Using this method, we perform molecular dynamics calculations and discuss the dynamic effect of molecular rotation on the structure of and binding in MAPbI₃, which allowed for rationalizing microscopically the simultaneous occurrence of cubic octahedral symmetry and MA disorder.

I. INTRODUCTION

In recent years, the hope of cheap, solution-based solar cells with efficiencies above 20% has fueled the scientific research in halide perovskites (HaPs).^{1–7} HaPs exhibit many interesting optoelectronic properties that make them ideal candidates for future semiconductor based applications, yet some of their structural and dynamic properties remain of central scientific interest since they also present major stumbling blocks in the development of stable devices. Fundamentally, HaPs can crystallize in the typical perovskite structure ABX_3 , where the B -site is a heavy metallic element such as lead, and halide ions (X) form octahedra centered around the B -site.⁸ In hybrid organic-inorganic HaPs, the voids between the inorganic scaffolds are occupied by the organic A -site (in this work methylammonium, MA). As is typical for perovskites, HaPs undergo phase transitions with changes in temperature. The prototypical variant MAPbI₃ has an orthorhombic symmetry up to 162 K, where it changes to a tetragonal structure. The second phase transition occurs at 327 K, where it switches to a cubic crystal structure.^{9,10} Importantly, HaPs are compared to other well established semiconductors¹¹ and perovskite materials very soft mechanically,^{12–17} which is interesting fundamentally and could become problematic when they are exposed to the operating conditions of commercially used solar cells. Furthermore, experimental and theoretical studies have also shown that the structure and binding in HaPs can be modified already by applying relatively low pressure.^{18–20} Therefore, it is interesting to study the interrelation of binding and structural modifications in HaPs, which can be induced by a change in temperature or applied pressure, and may have important consequences for their optoelectronic properties. Such insight can be generated from first-principles based com-

putations. However, from a theoretical point of view there are a number of physical effects and properties, all of which could play a role regarding the structure of and binding in HaPs. First, hybrid HaPs consist of highly polarizable atoms such as iodine and lead and contain hydrogen atoms bound to electronegative species (e.g. nitrogen); hence, from simple chemical arguments dispersive interactions, such as van der-Waals (vdW) and hydrogen bonding, can be expected to play an important role in HaPs. Several computational studies have shown that dispersive interactions are crucial in static calculations of the lattice constants and mechanical properties of HaPs.^{12,16,21–27} However, as to how their treatment for HaPs should best be implemented in density functional theory (DFT), the most widely used method for HaPs, is still an open question.^{28,29} In particular, a recent study has concluded that correcting for dispersive interactions in calculations of HaPs does not improve their description.³⁰ Second, Kohn-Sham DFT functionals, such as the frequently used generalized gradient approximation (GGA), cannot accurately describe the band gap of semiconductors even in principle,^{31,32} which can be improved by applying computationally more costly hybrid functionals in the generalized Kohn-Sham framework.^{33,34} For classical inorganic semiconductors, screened hybrid functionals were shown to improve also the description of lattice constants compared to GGA-based approaches.^{35–37} The question that naturally arises then is whether a similar improvement is found when using a hybrid functional for calculating the structure of HaPs, as has been suggested recently.³⁰ Third, it is well established that spin-orbit coupling (SOC) due to the presence of the lead atom in MAPbI₃ leads to strong modifications in the electronic structures, i.e., it lifts the degeneracy of the conduction and valence band and lowers the band gap.^{38,39} Lastly, since HaPs are mechanically soft, they exhibit large structural dynamical effects, such as massive ionic displacements and molecular rotation around room temperature,^{40,41} which is the relevant scenario for device applications. Therefore, it is important to investigate the

^{a)}Electronic mail: david.egger@physik.uni-regensburg.de

consequences of these unusual structural dynamical effects on the pertinent structural properties of HaPs. To the best of our knowledge, the impact of finite temperature on the lattice constants and mechanical properties, and the role of dispersive interactions in calculating them, has not been addressed by means of DFT-based molecular dynamics (MD).

In this study, we first investigate how the choice of vdW correction and DFT functional affects the results of calculations for structure and binding in the prototype MAPbI₃. To this end, we compare data obtained in static DFT calculations for a primitive cubic unit cell to experimental ones, using various computational approaches. The most promising choice of method is then used to explore how different MA orientations impact structural properties in static and finite-temperature MD calculations of MAPbI₃.

II. METHODS AND COMPUTATIONAL SETUP

A satisfactory treatment of dispersion forces within conventional approximate Kohn-Sham DFT functionals requires dispersive correction schemes. In our calculations, we considered the Tkatchenko-Scheffler method with regular Hirshfeld partitioning (TS)⁴² and with an iterative Hirshfeld partitioning (HI)^{43,44} as well as the many-body dispersion (MBD) method.^{45–47} The TS and HI methods include pairwise dispersive interactions between atoms in the crystal. The HI scheme expands the Hirshfeld partitioning with an iterative process that results in a more realistic allocation of charges for strongly ionic systems.⁴³ To include the screening of dispersive interactions that occurs in a many-body system, we apply the MBD method based on the random phase expression of the correlation energy, as developed by Tkatchenko et al.⁴⁵

For the comparison of results obtained by using a GGA functional and a hybrid functional, we apply two very common variants in the context of solid-state calculations, namely the PBE⁴⁸ and HSE functionals.^{49,50} In the HSE functional, the short-range exchange energy is calculated as a mix of PBE and exact exchange,^{49,50} which was often found to improve the description of electronic-structure and structural properties of semiconductors.^{35–37,51} SOC describes the interaction of the spin angular momentum with the orbital momentum, and it plays a crucial role in systems with heavy elements such as lead. In our calculations, it was described fully self-consistently within the framework of non-collinear magnetism,⁵² in conjunction with the various DFT methods applied here.

In order to obtain structural and mechanical parameters, we use an equation of state that accurately describes the macroscopic properties of the crystal. One of the most frequently used ones is the Birch-Murnaghan equation of state (BMEOS).^{53–55} It describes the free energy of a solid as a function of the volume of the unit cell, $E(V)$, at isothermal conditions as:

$$E(V) = E_0 + \frac{B_0 V}{B'_0} \left(\frac{(V_0/V)^{B'_0}}{B'_0 - 1} + 1 \right) - \frac{V_0 B_0}{B'_0 - 1}. \quad (1)$$

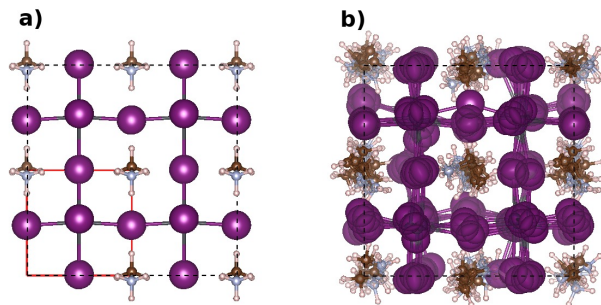


FIG. 1. Schematic structural representations of the configurations of MAPbI₃ that were used in the calculations: a) Primitive unit cell (red solid line) and a 2x2x2 supercell (black dashed line) used in static calculations; note that we have considered various orientations of MA, see text for details. b) Visualization of the structural changes in molecular dynamics (MD) calculation of a 2x2x2 supercell, which was obtained as an overlay of five structures separated by 200 fs along the 20 ps DFT-MD trajectory. Shown are carbon (brown), nitrogen (light blue), hydrogen (white), iodine (violet), and lead (gray) atoms. Atoms belonging to more than the computational cell are displayed for visual clarity.

E_0 is the free energy at the equilibrium volume, V_0 , and B_0 and B'_0 are the bulk modulus and its derivative, respectively. In order to obtain these parameters, we first calculate the free energy of the static system at eight equidistant volumes between 90% and 111% of the experimental value¹⁰ and fit Eq. 1 using these eight values (tests with more data points did not show any significant improvement) with the method of least squares. Note that while the E_0 and B'_0 are required to fit Eq. 1, they are not relevant for our discussion.

In our calculations, we first considered the cubic primitive unit cell of MAPbI₃ as has been reported experimentally, see Fig. 1a.¹⁰ To be able to also investigate the effect of MA orientation, we used a supercell that consists of eight unit-cells stacked together in a 2x2x2 pattern (see Fig. 1a), with the MA ions orientated in parallel or anti-parallel to each other. In this way, we can test the effect of the assumption that MA molecules are oriented perfectly in parallel throughout the material on computing the structural and binding properties of MAPbI₃. Note that in these calculations, the angle between the MA molecules was fixed during the atomic relaxation. To fit Eq. 1 with the data obtained in the MD calculations, the average free energy along a trajectory of 20 ps was calculated for each volume point, which was used, together with the standard deviation as the uncertainty, in the fit of Eq. 1. We note that since the fit errors of B' were quite large in the case of the MD calculations, in fitting Eq. 1 we set B' to the value obtained in the static calculation of the unit cell.

The DFT calculations were performed with a plane-wave basis (cutoff energy: 400 eV) and the projector-augmented wave (PAW) method,⁵⁸ as implemented in the VASP code.⁵⁹ For unit cell calculations, a 6x6x6 grid of k-points centered around the Γ -point was used, for static and dynamic calculations that considered the supercell, the grid was reduced to a sampling of 3x3x3. For each static calculation, the ionic co-

TABLE I. Volume of the primitive unit cell, V_0 , and bulk modulus, B_0 , obtained by fitting the DFT-calculated data with Eq. 1, using various methods applied to the primitive unit-cell of MAPbI₃.

	PBE	PBE+TS	PBE+MBD	PBE+HI	HSE	HSE+TS	HSE+MBD	HSE+HI	PBE+SOC	PBE+TS+SOC	Experiment
ine V_0 [\AA^3] ^a	272.9	256.2	257.1	262.0	266.6	252.9	252.1	258.1	274.4	256.3	247-253 ^{10,12,56}
B_0 [GPa] ^b	10.6	15.7	13.6	14.3	11.1	16.4	14.7	14.2	9.6	15.0	12-16 ^{14,57}

^a Errors are between 0.1 and 0.4 \AA^3

^b Errors are between 0.2 and 0.4 GPa

ordinates were relaxed, using the PBE functional and the respective dispersive correction scheme, with the Gadget tool in internal coordinates,⁶⁰ before calculating the energies to fit Eq. 1. In the calculations applying the HSE functional or SOC, the respective PBE-based geometry was used to reduce computational costs. For all static calculations, the geometry was considered relaxed when the forces acting on the atoms were below 10 meV per \AA . In the canonical (NVT) MD simulations, a MAPbI₃ 2x2x2 supercell with randomly orientated MA was used as a starting point for the structural geometry, in line with the recommendations provided by Lahnsteiner et al.⁶¹ It was then equilibrated for 5 ps and computed for 20 ps in time steps of 1 fs at a temperature of 400 K. This protocol is sufficient to compute the impact of the dynamic nuclear effects on the structure and binding despite the limited supercell size⁶¹ and trajectory length. The latter was checked explicitly by adding another 10 ps to the simulation, which resulted in only insignificant changes of the calculated observables. Schematic representations of the structures were generated with VESTA.⁶²

III. RESULTS

Fig. 2 shows the energy change due to volume change, i.e., $\Delta E(V) = E(V) - E_0$, for the static calculations of the MAPbI₃ unit cell, calculated by using the PBE and HSE functionals augmented by different dispersion corrections. The optimized volume (V_0) and bulk modulus (B_0), obtained from the fit, are listed in Table I. Considering the PBE data, it can readily be seen that using dispersive corrections has a large impact on the result. Furthermore, it was found that the results from the TS and MBD methods are very similar, and provide a V_0 of 256.2 \AA^3 (PBE+TS) and 257.1 \AA^3 (PBE+MBD) which are close to the experimental range of 247-253 \AA^3 . In contrast, the bare PBE calculations are far off (272.9 \AA^3) the experimental range, in agreement with literature findings,^{12,21-25} and the PBE+HI (262.0 \AA^3) results basically lie in between the results of bare PBE and PBE+TS/PBE+MBD. The calculated B_0 data show similar trends, i.e., the experimentally reported values (12-16 GPa) agree well with the PBE+TS, PBE+MBD, and PBE+HI results, but deviate more from the bare PBE value. From these data, one can see that the TS dispersive correction scheme with a regular Hirshfeld partitioning and the MBD approach perform best in reproducing structural and binding properties measured in experiments. It should be noted that the experimental data were recorded at elevated temperatures, at least at $T \approx 330$ K, while the cal-

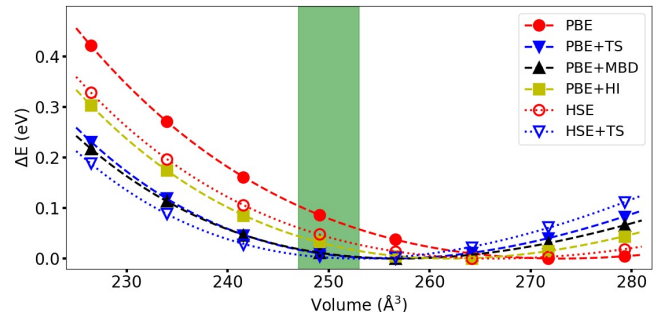


FIG. 2. Energy change as a function of unit-cell volume, $\Delta E(V) = E(V) - E_0$, for the static calculations of the primitive MAPbI₃ unit cell, using the PBE and HSE functionals augmented by different dispersion correction schemes. Also shown are fits to Eq. 1 and the range of experimental results for the volumes (green-shaded area). It is noted that a larger slope in the fit corresponds to a larger value of B_0 .

culations were performed at 0 K and do not address thermal expansion, an effect we discuss below based on our results obtained from finite-temperature MD calculations.

Fig. 2 also shows the results for regular and TS-corrected calculations using the HSE functional (see Table I for full dataset using the other correction schemes). While there is some visible difference between the PBE and HSE calculations without dispersive corrections, the bare HSE value for V_0 is still quite off the experimental result, in stark contrast to findings reported for conventional inorganic semiconductors.³⁵⁻³⁷ Considering the dispersion-corrected HSE data, it is found that these compare almost equally well to experiment as their PBE counterparts. Importantly, the optimized V_0 value using the PBE+TS, PBE+MBD, HSE+TS, and HSE+MBD are all within $< 5 \text{\AA}^3$, which is smaller than the range of experimentally reported values. Hence, we find that the improvement due to using the HSE functional is minor compared to using dispersive corrections, which is thus found to be the essential computational ingredient for obtaining accurate structural and binding properties of MAPbI₃. From these findings, we argue that using PBE+TS provides a reasonable choice for calculating structural and binding properties of HaPs such as MAPbI₃. For completeness, we note that calculations including SOC showed very little difference to those without, as can be seen in Table I.

It is well-known that the electronic interaction between MA and the inorganic ions in MAPbI₃ is minor, since the electronic states of MA are energetically not close to the band

TABLE II. Cell volume, V_0 , and bulk modulus, B_0 , obtained by fitting the DFT-calculated data with Eq. 1, using PBE and PBE+TS applied to a $2 \times 2 \times 2$ supercell of MAPbI_3 with differently orientated MA molecules. Note that in order to improve the comparison, we here report $V_0/8$.

	parallel MA		anti-parallel MA
ine		PBE	
$V_0 [\text{\AA}^3]^a$	272.9		267.5
$B_0 [\text{GPa}]^b$	10.8		11.2
		PBE+TS	
$V_0 [\text{\AA}^3]^a$	256.3		253.8
$B_0 [\text{GPa}]^b$	15.7		14.7

^a Errors are between 0.1 and 0.3 \AA^3

^b Errors are between 0.4 and 0.4 GPa

edges. Nevertheless, electrostatic and dispersive interactions between the inorganic ions and MA could still be important for the structure and binding of MAPbI_3 . In order to test this, we varied the MA orientation in a $2 \times 2 \times 2$ supercell, considering the extreme cases of either perfectly parallel or antiparallel MA molecules. It is noted that the former scenario is equivalent to considering a primitive cubic unit cell of MAPbI_3 containing one MA unit. When calculating the structural parameters of the $2 \times 2 \times 2$ supercell with different MA orientations, we limit the calculations to the bare PBE and the PBE+TS approach, since neither using HSE nor including SOC has shown a significant improvement that would justify the increase in computational cost (see above and Table I). Furthermore, using the TS and MBD dispersive correction scheme provided essentially equal results, but the computational costs associated with the MBD method increase more rapidly when the number of atoms becomes larger compared to the TS scheme.

The first relevant observation in the data shown in Table II is that the results of the supercell calculations considering the parallel MA orientation are, within the fitting error, identical to the results obtained with the calculations for the primitive unit cell, as expected. However, a noticeable difference occurs in both the structure (see Fig. 3) and the optimized parameters (see Table II) when the MA orientation is changed to the other extreme of perfectly antiparallel MA molecules. In the case of the parallel MA orientation, at all volumes the octahedra retain cubic symmetry, whereas in the antiparallel orientation they tilt strongly (see Fig. 3). Indeed, this effect is important, since for the fit of the supercell data calculated with bare PBE we find that $V_0/8$ changes from 272.7\AA^3 , for the parallel orientation, to 265.8\AA^3 , for the antiparallel one. The same trend is confirmed in the PBE+TS calculations, although the differences are smaller. Hence, the interaction between the inorganic cage and the MA molecules is important for the structure and binding in MAPbI_3 . Since our DFT calculations show that the antiparallel orientation is preferred in MAPbI_3 , i.e., the free energy is consistently lower for the antiparallel MA orientation at all eight volumes, this requires further investigations.

Hence, motivated by the finding that MA orientation impacts structure and binding in MAPbI_3 , we performed fully

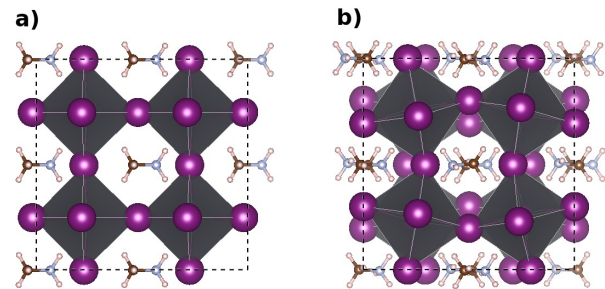


FIG. 3. Schematic representations of the supercells with optimized atomic geometries obtained with PBE+TS at a volume of 256.6\AA^3 , for the case of parallel (a) and antiparallel MA orientation (b). The x-z plane is shown, and atoms belonging to more than the computational cell are displayed for visual clarity

TABLE III. Cell volume, V_0 , and bulk modulus, B_0 , obtained by fitting the DFT-calculated data with Eq. 1, using PBE and PBE+TS applied to a $2 \times 2 \times 2$ supercell of MAPbI_3 computed along an MD trajectory of 20 ps. Note that in order to improve the comparison, we here report $V_0/8$.

	PBE	PBE+TS
ine $V_0 [\text{\AA}^3]^a$	267.3	248.1
$B_0 [\text{GPa}]^a$	8.8	13.0

^a Errors are 0.1 \AA^3

^b Errors are between 0.6 and 0.7 GPa

unconstrained NVT MD calculations at 400 K. This is relevant, since the MA unit was found to be only weakly bound in the cubic phase,^{63,64} and hence undergoes rotational and translational motion at elevated temperatures, which could impact the energetics in the material dynamically. Furthermore, the MD calculations allow for testing whether the effect of dispersive corrections seen for the static structures is still visible at elevated temperatures, a comparison that has not been attempted previously but is important for investigating dynamical effects in the structural interaction of MAPbI_3 . Fig. 4 shows the entire distribution as well as the mean value of the PBE- and PBE+TS-calculated change in free energy of MAPbI_3 , ΔE , determined for a 20 ps MD simulation, again fitted by Eq. 1. The most apparent finding from Fig. 4 is yet again the sizable difference between the PBE and PBE+TS curves, as also quantified by the V_0 parameters provided in Table III. Furthermore, a slight decrease of V_0 is found in the MD calculations at 400 K compared to the static 0 K calculation, contrary to the expected thermal expansion. In regard to B_0 , while in the case of PBE it is similar to the 0 K calculation of the primitive unit cell, for PBE+TS B_0 it is slightly lower than what was obtained in the static calculations.

In order to better understand the origin of these findings, the average atomic positions along the PBE+TS MD trajectories were calculated. Fig. 5 shows that depending on the volume of the supercell, two different types of structures emerged. For the three smallest volumes considered in the MD, the octa-

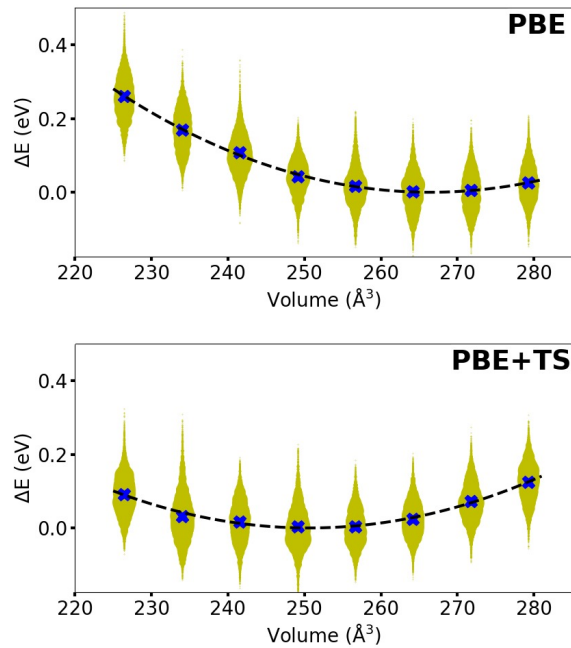


FIG. 4. Energy change as a function of unit-cell volume, $\Delta E(V) = E(V) - E_0$, calculated by using MD-DFT with PBE (top) and PBE+TS (bottom) along a trajectory of 20 ps, shown as yellow dots, where the symbol size is given by number of occurrences in the MD run. The blue cross denotes the average $\Delta E(V)$, and the black dashed line is the fit according to Eq. 1. Note that in order to improve the comparison, we here report $\Delta E/8$ as a function of $V/8$.

hedra were found to be tilted and the C-N bond of MA is still clearly visible in the average structure: successive MA molecules are oriented in parallel to each other along one direction and orthogonal to each other in the other two directions, aligning with the long axis of the rhombus created by the tilted octahedra. For the five larger considered volumes, on the other hand, the octahedra form an on average near perfect cubic symmetry, and the average carbon and nitrogen atoms are almost conjoined. The latter could either mean that there is absolutely no preferred direction of the MA molecules, i.e., it rotates such that it is entirely disordered over the course of the 20 ps trajectory, or that there are preferred directions which are equally occupied thermally.

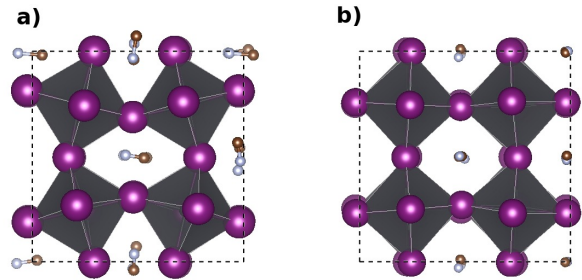


FIG. 5. Schematic representation of the time-averaged atomic positions along the MD trajectory, calculated with PBE+TS, for $V_0 = 231.0 \text{\AA}^3$ (a) and 256.6\AA^3 (b). Note that hydrogen atoms were omitted for clarity.

IV. DISCUSSION

The results from the static unit cell calculations confirmed previous findings that showed the importance of including dispersive interaction in DFT calculations for the structure and binding in MAPbI₃.^{12,21–25} Here, we went beyond in testing a range of dispersive-correction schemes: PBE calculations corrected by the TS scheme with the regular Hirshfeld partitioning and the MBD scheme showed good agreement with experimental data. The TS method with iterative Hirshfeld partitioning performed slightly worse than the regular TS and MBD schemes. While the iterative Hirshfeld partitioning has indeed been shown to improve the description of ionic materials,^{43,44} MAPbI₃ is a more complex case, since it is a hybrid organic-inorganic system that contains covalent bonds (in the MA molecule) as well as partially covalent-ionic bonds (in the inorganic framework). One perhaps surprising result is that the MBD method did not improve the results significantly compared to the TS method, even though one would expect that the iodine atoms, which account for most of the vdW-interactions,²² are screened by the surrounding dielectric environment. We considered a comparison of the C_6 parameters calculated from PBE+TS and PBE+MBD, which determine the dispersive correction in either case,^{28,29} to further understand this result. We find that the changes are minor, on the order of 1 % or smaller, and furthermore do not depend on the volume of the unit cell. This implies that the screening is barely affected by the changes in distance in the calculations at different volumes, and thereby only leads to a constant energy shift. Furthermore, we considered the higher-order contributions to the dispersive energy calculated with PBE+MBD, to find that indeed the second-order term is dominating. This could imply that the dispersive interactions in MAPbI₃ are such that higher-order interactions are indeed negligible compared to the pairwise contribution, and also that the polarizability is largely isotropic (see ref.²⁹ for further discussion).

Furthermore, we found that using the hybrid functional HSE, which improves the description of the electronic structure, did not result in improvements for the optimized unit-

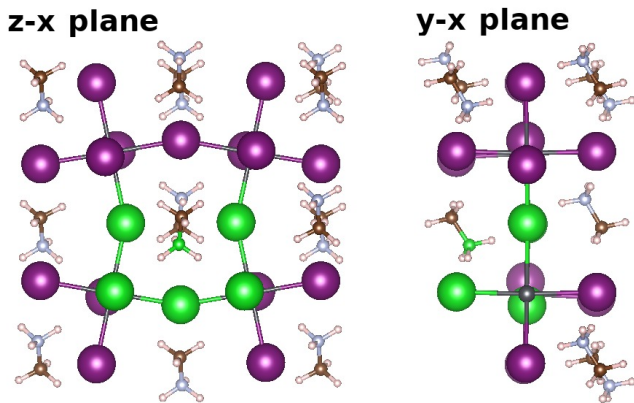


FIG. 6. Schematic representation of the interaction between the ammonium-end of MA and the surrounding iodine atoms; the relevant atoms are highlighted in green, and the z-x plane (left) and y-x plane (right) are shown. The structure is taken from the PBE+TS calculation of $V = 256.6 \text{ \AA}^3$ as visualized in Fig. 3.

cell volume and bulk modulus, once it was combined with dispersive corrections. Indeed, the results from the PBE+TS, PBE+MBD, HSE+TS, and HSE+MBD calculations are all within experimentally reported range for these two important structural parameters. Since our data, presented in Table I, also confirm the effect of SOC for the structure and binding to be minor, and since the PBE+TS approach was shown to be very accurate for structural and mechanical properties of multiple HaP crystals,^{16,22–24,26,27} we conclude that using PBE+TS for investigating the structure and binding in static and dynamical calculations of HaPs is a reasonable choice.

In this context, it is worth noting that Bokdam *et al.*³⁰ suggested the choice of DFT functional to have a bigger impact on the structural properties of MAPbI₃ than the addition of dispersive corrections. While this is certainly true for electronic properties, and while our calculations showed some minor differences between the PBE and HSE results, we have shown that this clearly cannot diminish the important role of dispersive interactions in MAPbI₃. We further note that the different conclusions of our work and Bokdam *et al.*³⁰ could be related to the different points of reference used in either case: while we have chosen to consider experimental data on the lattice constants and bulk modulus, Bokdam *et al.*³⁰ considered energies calculated in the random-phase approximation (RPA) as a reference. Indeed, RPA energies can be very accurate for solids and are broadly applicable, but it is worth noting that “standard” RPA suffers from known deficiencies, such as potentially incorrect descriptions of short-range correlation.^{29,65}

Using the PBE+TS approach allowed for studying more complicated static and dynamic structural phenomena: First, we investigated the impact of MA orientation on the structural parameters of MAPbI₃, studying the extreme cases of either perfectly parallel or antiparallel MA molecules contained in a supercell. We found that only for the parallel orientation of MA do the octahedra retain cubic symmetry, while for antiparallel MA molecules they strongly tilt. Note that the lat-

tice vectors were still constrained to the primitive unit cell, i.e., the volume change corresponds to a hydrostatic pressure in the system. Since the relative energy gain/cost due to these structural distortions depends on the unit-cell volume, this effect modified the obtained volume and bulk modulus. Hence, the interaction between MA and the inorganic atoms is important, especially because the calculations showed that the antiparallel orientations are actually energetically preferred.

The origin of these distortions is related to the interactions between the MA molecules and iodine atoms, since the partially positive ammonium-part of the MA interacts stronger with the partially negatively iodide ion than the methyl-side. In Fig. 6 we illustrate that the nitrogen atoms of MA interact mainly with five of the neighboring iodines, which results in a distortion of the octahedra such that the distances between the nitrogen and iodine atoms are maintained between 3.64 and 3.81 Å. These interactions seem to be the main driving force behind the MA-induced distortions of the octahedra in the antiparallel case, which are energetically favorable for the system. Due to symmetry, these interactions are cancelled in the case of parallel MA orientation, and our geometry relaxations did not automatically adapt to the more favorable antiparallel scenario. This finding is also quite interesting in view of the fact that the experimentally-determined lattice symmetry of MAPbI₃ above 327 K is almost perfectly cubic,^{9,10} despite the fact that different MA orientations can induce lower energy structures.

The implications of these findings can be fully understood by means of fully-unconstrained MD calculations at 400 K, since in these the MA molecules, as well as all other atoms, are allowed to move freely. The first important finding from these data was that inclusion of dispersive corrections is equally important to obtain reasonable structural parameters in MD calculations. Second, the results obtained from the MD simulations are quite surprising at first sight, since the unit-cell volume was found to be smaller than the one obtained from the 0 K static calculation. To understand this finding, consider that the time-scales associated with MA motion are much faster than the ones corresponding to the octahedral distortions of the heavy Pb-I cage, which is included in the MD but absent in the static calculations. Our analysis further showed that the average nuclear positions of MA are such that the carbon and nitrogen atoms are essentially conjoined at this temperature, meaning that MA is disordered, which is well known.⁹ Hence, the inorganic atoms essentially respond to a time-averaged volume corresponding to the moving MA molecule. Due to the MA disorder, this volume is effectively smaller at 400 K than for a fixed pattern of MA orientations, allowing for shorter I-Pb-I bonds and hence smaller crystal volumes. Last but not least, this rationale also explains the finding from the MD data showing that the time-averaged octahedral symmetry is almost perfectly cubic at 400 K in agreement with experiment: MA disorder implies that all possible octahedral distortions induced by MA-iodine interactions are statistically equally likely. Therefore, the cubic perovskite structure is maintained as the most energetically favorable average crystal structure, exhibiting all the electronic and optical properties that render MAPbI₃ so favorable for device appli-

cations.

Finally, the data contained in Fig. 5 showed that at smaller volumes the MD-averaged nuclear positions exhibit octahedral distortions together with a more preferred orientational order of MA. This makes sense, considering that smaller unit-cell volumes correspond to smaller voids between the octahedra, which increases the organic-inorganic interactions,²⁴ and partially hinders free MA motion. Such tilting of the octahedra into an orthorhombic-like structure was also observed experimentally in pressure experiments¹⁸ for MAPbI₃, and the variation in the preferred direction for MA at different volumes was discussed also in a recent study reporting MD simulations.⁶⁶ Therefore, in agreement with previous findings our study shows that even relatively mild changes in external pressure can result in large changes of the structure and binding in MAPbI₃.

V. CONCLUSION

In summary, we investigated the impact of various levels of DFT-related approximations for calculations of the structural and binding properties of the prototypical HaP material MAPbI₃. Our tests considered the effects of including different dispersive correction schemes, applying a hybrid functional, including SOC, and also addressed the role of dynamic effects in MD calculations. The data confirmed previous theoretical work showing that dispersive corrections are important for accurate calculations of MAPbI₃, and also highlight that applying a computationally much more expensive hybrid functional improves the description of structural and mechanical properties by only a small amount. From this, we conclude that the use of a semilocal functional, augmented by pairwise dispersive interactions, is a suitable choice when computing more complicated static as well as structural dynamical phenomena in HaPs. Applying this methodology to DFT-based MD calculations of MAPbI₃, we analyzed the dynamic effect of molecular motion and its interplay with the structure of and binding in MAPbI₃. From this analysis, we could rationalize microscopically the simultaneous occurrence of a preferred cubic octahedral symmetry and MA disorder.

VI. ACKNOWLEDGEMENTS

Funding provided by the Alexander von Humboldt Foundation in the framework of the Sofja Kovalevskaja Award endowed by the German Federal Ministry of Education and Research is acknowledged. The authors gratefully acknowledge the Gauss Centre for Supercomputing e.V. (www.gauss-centre.eu) for funding this project by providing computing time through the John von Neumann Institute for Computing (NIC) on the GCS Supercomputer JUWELS at Jülich Supercomputing Centre (JSC).

VII. REFERENCES

- N.-G. Park, "Organometal perovskite light absorbers toward a 20% efficiency low-cost solid-state mesoscopic solar cell," *The Journal of Physical Chemistry Letters* **4**, 2423–2429 (2013), <https://doi.org/10.1021/jz400892a>.
- H. J. Snaith, "Perovskites: The emergence of a new era for low-cost, high-efficiency solar cells," *The Journal of Physical Chemistry Letters* **4**, 3623–3630 (2013), <https://doi.org/10.1021/jz4020162>.
- S. Kazim, M. K. Nazeeruddin, M. Grätzel, and S. Ahmad, "Perovskite as light harvester: A game changer in photovoltaics," *Angewandte Chemie International Edition* **53**, 2812–2824 (2014), <https://onlinelibrary.wiley.com/doi/pdf/10.1002/anie.201308719>.
- S. D. Stranks and H. J. Snaith, "Metal-halide perovskites for photovoltaic and light-emitting devices," *Nature nanotechnology* **10**, 391 (2015).
- F. Zheng, D. Saldana-Greco, S. Liu, and A. M. Rappe, "Material innovation in advancing organometal halide perovskite functionality," *The Journal of Physical Chemistry Letters* **6**, 4862–4872 (2015), pMID: 26631361, <https://doi.org/10.1021/acs.jpcllett.5b01830>.
- T. M. Brenner, D. A. Egger, L. Kronik, G. Hodes, and D. Cahen, "Hybrid organic–inorganic perovskites: low-cost semiconductors with intriguing charge-transport properties," *Nature Reviews Materials* **1**, 15007 (2016).
- W. Li, Z. Wang, F. Deschler, S. Gao, R. H. Friend, and A. K. Cheetham, "Chemically diverse and multifunctional hybrid organic–inorganic perovskites," *Nature Reviews Materials* **2**, 16099 (2017).
- B. Saparov and D. B. Mitzi, "Organic–inorganic perovskites: Structural versatility for functional materials design," *Chemical Reviews* **116**, 4558–4596 (2016), pMID: 27040120, <https://doi.org/10.1021/acs.chemrev.5b00715>.
- A. Poglitsch and D. Weber, "Dynamic disorder in methylammoniumtrihalogenoplumbates (ii) observed by millimeter-wave spectroscopy," *The Journal of Chemical Physics* **87**, 6373–6378 (1987), <https://doi.org/10.1063/1.453467>.
- C. C. Stoumpos, C. D. Malliakas, and M. G. Kanatzidis, "Semiconducting tin and lead iodide perovskites with organic cations: Phase transitions, high mobilities, and near-infrared photoluminescent properties," *Inorganic Chemistry* **52**, 9019–9038 (2013), pMID: 23834108, <https://doi.org/10.1021/ic401215x>.
- D. A. Egger, A. Bera, D. Cahen, G. Hodes, T. Kirchartz, L. Kronik, R. Lovrincic, A. M. Rappe, D. R. Reichman, and O. Yaffe, "What remains unexplained about the properties of halide perovskites?" *Advanced Materials* **30**, 1800691 (2018), <https://onlinelibrary.wiley.com/doi/pdf/10.1002/adma.201800691>.
- J. Feng, "Mechanical properties of hybrid organic-inorganic CH₃NH₃BX₃ (B = Sn, Pb; X = Br, I) perovskites for solar cell absorbers," *Apl Materials* **2**, 081801 (2014).
- S. Sun, Y. Fang, G. Kieslich, T. J. White, and A. K. Cheetham, "Mechanical properties of organic–inorganic halide perovskites, CH₃NH₃PbX₃ (X = I, Br and Cl), by nanoindentation," *Journal of Materials Chemistry A* **3**, 18450–18455 (2015).
- Y. Rakita, S. R. Cohen, N. K. Kedem, G. Hodes, and D. Cahen, "Mechanical properties of APbX₃ (A = Cs or CH₃NH₃; X = I or Br) perovskite single crystals," *MRS Communications* **5**, 623–629 (2015).
- A. Létoublon, S. Paofai, B. Rufflé, P. Bourges, B. Hehlen, T. Michel, C. Ecolivet, O. Durand, S. Cordier, C. Katan, and J. Even, "Elastic constants, optical phonons, and molecular relaxations in the high temperature plastic phase of the CH₃NH₃PbBr₃ hybrid perovskite," *The Journal of Physical Chemistry Letters* **7**, 3776–3784 (2016), pMID: 27601100, <https://doi.org/10.1021/acs.jpcllett.6b01709>.
- I. V. Kabakova, I. Azuri, Z. Chen, P. K. Nayak, H. J. Snaith, L. Kronik, C. Paterson, A. A. Bakulin, and D. A. Egger, "The effect of ionic composition on acoustic phonon speeds in hybrid perovskites from Brillouin spectroscopy and density functional theory," *Journal of Materials Chemistry C* **6**, 3861–3868 (2018).
- G. A. Elbaz, W.-L. Ong, E. A. Doud, P. Kim, D. W. Paley, X. Roy, and J. A. Malen, "Phonon speed, not scattering, differentiates thermal transport in lead halide perovskites," *Nano Letters* **17**, 5734–5739 (2017), pMID: 28806090, <https://doi.org/10.1021/acs.nanolett.7b02696>.
- F. Capitani, C. Marini, S. Caramazza, P. Postorino, G. Garbarino, M. Hanfland, A. Pisanu, P. Quadrelli, and L. Malavasi, "High-pressure behavior

- of methylammonium lead iodide (MAPbI₃) hybrid perovskite,” *Journal of Applied Physics* **119**, 185901 (2016), <https://doi.org/10.1063/1.4948577>.
- ¹⁹J. A. Flores-Livas, D. Tomerini, M. Amsler, A. Boziki, U. Rothlisberger, and S. Goedecker, “Emergence of hidden phases of methylammonium lead iodide CH₃NH₃PbI₃ upon compression,” *Physical Review Materials* **2**, 085201 (2018).
 - ²⁰L. Zhang, Q. Zeng, and K. Wang, “Pressure-induced structural and optical properties of inorganic halide perovskite CsPbBr₃,” *The Journal of Physical Chemistry Letters* **8**, 3752–3758 (2017), pMID: 28742359, <https://doi.org/10.1021/acs.jpcclett.7b01577>.
 - ²¹Y. Wang, T. Gould, J. F. Dobson, H. Zhang, H. Yang, X. Yao, and H. Zhao, “Density functional theory analysis of structural and electronic properties of orthorhombic perovskite CH₃NH₃PbI₃,” *Physical Chemistry Chemical Physics* **16**, 1424–1429 (2013).
 - ²²D. A. Egger and L. Kronik, “Role of dispersive interactions in determining structural properties of organic–inorganic halide perovskites: insights from first-principles calculations,” *The journal of physical chemistry letters* **5**, 2728–2733 (2014).
 - ²³C. Motta, F. El-Mellouhi, S. Kais, N. Tabet, F. Alharbi, and S. Sanvito, “Revealing the role of organic cations in hybrid halide perovskite CH₃NH₃PbI₃,” *Nature communications* **6**, 7026 (2015).
 - ²⁴J. Li and P. Rinke, “Atomic structure of metal-halide perovskites from first principles: The chicken-and-egg paradox of the organic–inorganic interaction,” *Physical Review B* **94**, 045201 (2016).
 - ²⁵M. Faghinihasiri, M. Izadifard, and M. E. Ghazi, “DFT study of mechanical properties and stability of cubic methylammonium lead halide perovskites (CH₃NH₃PbX₃, X = I, Br, Cl),” *The Journal of Physical Chemistry C* **121**, 27059–27070 (2017), <https://doi.org/10.1021/acs.jpcc.7b07129>.
 - ²⁶C. Motta, F. El-Mellouhi, and S. Sanvito, “Exploring the cation dynamics in lead-bromide hybrid perovskites,” *Physical Review B* **93**, 235412 (2016).
 - ²⁷D. A. Egger, “Intermediate bands in zero-dimensional antimony halide perovskites,” *The Journal of Physical Chemistry Letters* **9**, 4652–4656 (2018), pMID: 30052447, <https://doi.org/10.1021/acs.jpcclett.8b01730>.
 - ²⁸L. Kronik and A. Tkatchenko, “Understanding molecular crystals with dispersion-inclusive density functional theory: Pairwise corrections and beyond,” *Accounts of Chemical Research* **47**, 3208–3216 (2014), pMID: 24901508, <https://doi.org/10.1021/ar500144s>.
 - ²⁹J. Hermann, R. A. DiStasio, and A. Tkatchenko, “First-principles models for van der waals interactions in molecules and materials: Concepts, theory, and applications,” *Chemical Reviews* **117**, 4714–4758 (2017), pMID: 28272886, <https://doi.org/10.1021/acs.chemrev.6b00446>.
 - ³⁰M. Bokdam, J. Lahnsteiner, B. Ramberger, T. Schäfer, and G. Kresse, “Assessing density functionals using many body theory for hybrid perovskites,” *Phys. Rev. Lett.* **119**, 145501 (2017).
 - ³¹J. P. Perdew and M. Levy, “Physical content of the exact kohn–sham orbital energies: Band gaps and derivative discontinuities,” *Phys. Rev. Lett.* **51**, 1884–1887 (1983).
 - ³²L. J. Sham and M. Schlüter, “Density-functional theory of the energy gap,” *Phys. Rev. Lett.* **51**, 1888–1891 (1983).
 - ³³A. Seidl, A. Görling, P. Vogl, J. A. Majewski, and M. Levy, “Generalized kohn–sham schemes and the band-gap problem,” *Physical Review B* **53**, 3764–3774 (1996).
 - ³⁴G.-X. Zhang, A. Tkatchenko, J. Paier, H. Appel, and M. Scheffler, “van der waals interactions in ionic and semiconductor solids,” *Physical Review Letters* **107**, 245501 (2011).
 - ³⁵J. Heyd and G. E. Scuseria, “Efficient hybrid density functional calculations in solids: Assessment of the heyd–scuseria–ernzerhof screened coulomb hybrid functional,” *The Journal of Chemical Physics* **121**, 1187–1192 (2004), <https://doi.org/10.1063/1.1760074>.
 - ³⁶J. Paier, M. Marsman, K. Hummer, G. Kresse, I. C. Gerber, and J. G. Ángyán, “Screened hybrid density functionals applied to solids,” *The Journal of Chemical Physics* **124**, 154709 (2006), <https://doi.org/10.1063/1.2187006>.
 - ³⁷M. Marsman, J. Paier, A. Stroppa, and G. Kresse, “Hybrid functionals applied to extended systems,” *Journal of Physics: Condensed Matter* **20**, 064201 (2008).
 - ³⁸J. Even, L. Pedesseau, J.-M. Jancu, and C. Katan, “Importance of spin–orbit coupling in hybrid organic/inorganic perovskites for photovoltaic applications,” *The Journal of Physical Chemistry Letters* **4**, 2999–3005 (2013), <https://doi.org/10.1021/jz401532q>.
 - ³⁹L. D. Whalley, J. M. Frost, Y.-K. Jung, and A. Walsh, “Perspective: Theory and simulation of hybrid halide perovskites,” *The Journal of Chemical Physics* **146**, 220901 (2017), <https://doi.org/10.1063/1.4984964>.
 - ⁴⁰J. M. Frost and A. Walsh, “What is moving in hybrid halide perovskite solar cells?” *Accounts of Chemical Research* **49**, 528–535 (2016), pMID: 26859250, <https://doi.org/10.1021/acs.accounts.5b00431>.
 - ⁴¹D. A. Egger, A. M. Rappe, and L. Kronik, “Hybrid organic–inorganic perovskites on the move,” *Accounts of Chemical Research* **49**, 573–581 (2016), pMID: 26878152, <https://doi.org/10.1021/acs.accounts.5b00540>.
 - ⁴²A. Tkatchenko and M. Scheffler, “Accurate molecular van der waals interactions from ground-state electron density and free-atom reference data,” *Physical Review Letters* **102**, 073005 (2009).
 - ⁴³T. Bučko, S. Lebègue, J. G. Ángyán, and J. Hafner, “Extending the applicability of the tkatchenko–scheffler dispersion correction via iterative hirschfeld partitioning,” *The Journal of Chemical Physics* **141**, 034114 (2014), <https://doi.org/10.1063/1.4890003>.
 - ⁴⁴T. Bučko, S. Lebègue, J. Hafner, and J. G. Ángyán, “Improved density dependent correction for the description of london dispersion forces,” *Journal of Chemical Theory and Computation* **9**, 4293–4299 (2013), pMID: 26589148, <https://doi.org/10.1021/ct400694h>.
 - ⁴⁵A. Tkatchenko, R. A. DiStasio, R. Car, and M. Scheffler, “Accurate and efficient method for many-body van der waals interactions,” *Physical Review Letters* **108**, 236402 (2012).
 - ⁴⁶A. Ambrosetti, A. M. Reilly, R. A. DiStasio, and A. Tkatchenko, “Long-range correlation energy calculated from coupled atomic response functions,” *The Journal of Chemical Physics* **140**, 18A508 (2014), <https://doi.org/10.1063/1.4865104>.
 - ⁴⁷T. Bučko, S. Lebègue, T. Gould, and J. G. Ángyán, “Many-body dispersion corrections for periodic systems: an efficient reciprocal space implementation,” *Journal of Physics: Condensed Matter* **28**, 045201 (2016).
 - ⁴⁸J. P. Perdew, K. Burke, and M. Ernzerhof, “Generalized gradient approximation made simple,” *Physical Review Letters* **77**, 3865–3868 (1996).
 - ⁴⁹J. Heyd, G. E. Scuseria, and M. Ernzerhof, “Hybrid functionals based on a screened coulomb potential,” *The Journal of Chemical Physics* **118**, 8207–8215 (2003), <https://doi.org/10.1063/1.1564060>.
 - ⁵⁰J. Heyd, G. E. Scuseria, and M. Ernzerhof, “Erratum: “hybrid functionals based on a screened coulomb potential” [j. chem. phys. 118, 8207 (2003)],” *The Journal of Chemical Physics* **124**, 219906 (2006), <https://doi.org/10.1063/1.2204597>.
 - ⁵¹B. G. Janesko, T. M. Henderson, and G. E. Scuseria, “Screened hybrid density functionals for solid-state chemistry and physics,” *Physical Chemistry Chemical Physics* **11**, 443–454 (2009).
 - ⁵²D. Hobbs, G. Kresse, and J. Hafner, “Fully unconstrained noncollinear magnetism within the projector augmented-wave method,” *Physical Review B* **62**, 11556–11570 (2000).
 - ⁵³F. Birch, “Finite elastic strain of cubic crystals,” *Physical Review* **71**, 809–824 (1947).
 - ⁵⁴F. D. Murnaghan, “The compressibility of media under extreme pressures,” *Proceedings of the National Academy of Sciences* **30**, 244–247 (1944), <https://www.pnas.org/content/30/9/244.full.pdf>.
 - ⁵⁵C. L. Fu and K. M. Ho, “First-principles calculation of the equilibrium ground-state properties of transition metals: Applications to Nb and Mo,” *Physical Review B* **28**, 5480–5486 (1983).
 - ⁵⁶T. Baikie, Y. Fang, J. M. Kadro, M. Schreyer, F. Wei, S. G. Mhaisalkar, M. Graetzel, and T. J. White, “Synthesis and crystal chemistry of the hybrid perovskite (CH₃NH₃)PbI₃ for solid-state sensitized solar cell applications,” *Journal of Materials Chemistry A* **1**, 5628–5641 (2013).
 - ⁵⁷A. Ferreira, A. Létoublon, S. Paofai, S. Raymond, C. Ecolivet, B. Rufflé, S. Cordier, C. Katan, M. I. Saidaminov, A. Zhumekenov, *et al.*, “Elastic softness of hybrid lead halide perovskites,” *arXiv preprint arXiv:1801.08701* (2018).
 - ⁵⁸G. Kresse and D. Joubert, “From ultrasoft pseudopotentials to the projector augmented-wave method,” *Phys. Rev. B* **59**, 1758–1775 (1999).
 - ⁵⁹G. Kresse and J. Furthmüller, “Efficient iterative schemes for ab initio total-energy calculations using a plane-wave basis set,” *Physical Review B* **54**, 11169–11186 (1996).
 - ⁶⁰T. Bučko, J. Hafner, and J. G. Ángyán, “Geometry optimization of periodic systems using internal coordinates,” *The Journal of Chemical Physics* **122**, 124508 (2005), <https://doi.org/10.1063/1.1864932>.

- ⁶¹J. Lahnsteiner, G. Kresse, A. Kumar, D. D. Sarma, C. Franchini, and M. Bokdam, "Room-temperature dynamic correlation between methylammonium molecules in lead-iodine based perovskites: An ab initio molecular dynamics perspective," *Physical Review B* **94**, 214114 (2016).
- ⁶²K. Momma and F. Izumi, "Vesta: a three-dimensional visualization system for electronic and structural analysis," *Journal of Applied Crystallography* **41**, 653–658 (2008).
- ⁶³T. Chen, B. J. Foley, B. Ipek, M. Tyagi, J. R. Copley, C. M. Brown, J. J. Choi, and S.-H. Lee, "Rotational dynamics of organic cations in the $\text{CH}_3\text{NH}_3\text{PbI}_3$ perovskite," *Physical Chemistry Chemical Physics* **17**, 31278–31286 (2015).
- ⁶⁴J. Li, M. Bouchard, P. Reiss, D. Aldakov, S. Pouget, R. Demadrille, C. Aumaitre, B. Frick, D. Djurado, M. Rossi, and P. Rinke, "Activation energy of organic cation rotation in $\text{CH}_3\text{NH}_3\text{PbI}_3$ and $\text{CD}_3\text{NH}_3\text{PbI}_3$: Quasi-elastic neutron scattering measurements and first-principles analysis including nuclear quantum effects," *The Journal of Physical Chemistry Letters* **9**, 3969–3977 (2018), pMID: 29961330, <https://doi.org/10.1021/acs.jpcllett.8b01321>.
- ⁶⁵J. Toulouse, I. C. Gerber, G. Jansen, A. Savin, and J. G. Ángyán, "Adiabatic-connection fluctuation-dissipation density-functional theory based on range separation," *Physical Review Letters* **102**, 096404 (2009).
- ⁶⁶J. Lahnsteiner, G. Kresse, J. Heinen, and M. Bokdam, "Finite-temperature structure of the MAPbI_3 perovskite: Comparing density functional approximations and force fields to experiment," *Physical Review Materials* **2**, 073604 (2018).